JTTEE5 19:1024–1031
DOI: 10.1007/s11666-010-9506-z
1059-9630/$19.00 © ASM International

The Effect of Substrate Surface Oxides on the Bonding of NiCr Alloy Particles HVAF Thermally Sprayed onto Aluminum Substrates

W. Trompetter, M. Hyland, D. McGrouther, P. Munroe, and A. Markwitz

(Submitted November 26, 2009; in revised form April 6, 2010)

The effect of substrate surface oxides on splat-substrate bonding was investigated by thermally spraying NiCr particles onto aluminum substrates with surface oxide layers grown hydrothermally and electrochemically. Cross sections of bonded solid and molten splats revealed substantial deformation of both the substrate and the surface oxide. In spite of the substantial substrate deformation, there was no significant loss of the surface oxide material and there was no observed diffusion of the substrate oxide into the NiCr particle or vice versa. For solid splats, the substrate oxide was still present over the entire splat-substrate interface, however for molten splats, the oxide had been penetrated in several locations allowing close proximity of the splat metal to the substrate metal. These results strengthen the theory that oxide layers impede bonding and that successful bonding occurs only when the surface oxide is substantially deformed or disrupted to produce mechanically interlocking features at the interface.

Keywords oxide, HVAF, splat-substrate bonding, splat-substrate interaction

1. Introduction

The role of the surface oxide on interfacial bonding of solid splats in high-velocity thermal spray coatings has been discussed by several researchers (Ref 1-3). They have observed that successful solid splat bonding occurs only above certain critical velocities. Van Steenkiste et al. (Ref 4) suggested that fracturing (or deformation) of surface oxide layers on both the incident particle and on the substrate becomes a necessary part of coating formation (via mechanical bonding) and that the incident velocity must be sufficiently high for this to occur. Then, interdiffusion or metallurgical bonding is possible once the surface oxide on the substrate and on the coating material has been disrupted. For molten particles, the surface oxide has also been shown to affect the spreading characteristics of the splats (Ref 5).

W. Trompetter, National Isotope Centre, GNS Science, Lower Hutt, New Zealand and Department of Chemical and Materials Engineering, University of Auckland, Auckland, New Zealand; **A. Markwitz**, National Isotope Centre, GNS Science, Lower Hutt, New Zealand; **M. Hyland**, Department of Chemical and Materials Engineering, University of Auckland, Auckland, New Zealand; and **D. McGrouther** and **P. Munroe**, Electron Microscope Unit, University of New South Wales, Sydney, NSW 2052, Australia. Contact e-mail: b.trompetter@gns.cri.nz.

Native oxides on both metal substrates and the NiCr powders are typically in the region of 1-30 nm (Ref 6, 7). Such thin oxide layers, because of their low thickness, prevent their effect on splat-substrate bonding from being fully investigated by microscopy techniques. To study the effect of the substrate surface oxide in detail, NiCr alloy particles were thermally sprayed using the high-velocity air-fuel (HVAF) technique onto aluminum substrates prepared using two different oxidation methods. Individual splats were investigated in detail to search for alterations of the oxide layer from the impact to determine how this affects splat bonding to the substrate.

2. Experimental Procedure

2.1 Substrate Surface Preparation

Oxidized aluminum substrates were prepared using the hydrothermal and electrochemical oxide pretreatment methods for growing surface oxide layers on polished aluminum substrates (mirror finish). The hydrothermal oxide was prepared by boiling a degreased aluminum substrate in de-ionized water for 4 h (Ref 8). The electrochemical oxide was prepared by electrolyzing a degreased aluminum substrate for 25 min at 20 V DC in 40 g L^{-1} H_3PO_4, at room temperature (Ref 9).

2.2 How Splats were Made

To study the effect of the substrate surface oxide layers on splat-substrate bonding in thermal spray coatings, oxidized substrates were thermally sprayed with commercial

NiCr alloy powder (Ni80/Cr20, 5-45 μm) supplied from Sulzer Metco using the HVAF technique (Ref 10). A Browning Aerospray (150 model) gun was operated with a chamber pressure of 325 kPa (47 psi) and a gun-substrate spray distance of 15 cm. Single splat samples were achieved by passing the HVAF gun across the substrate at a speed of 25 cm s^{-1}. To ensure that identical spray conditions where used for each substrate sample, the substrates (with dimensions 100 mm × 30 mm) were sprayed at the same time with the same pass of the gun.

2.3 How the Oxides and Splats were Analyzed

The single splats were investigated with a focused ion beam (FIB) microscope and cross-sectional SEM. The FEI xP200 (FEI, Portland, OR) FIB (Ref 11, 12) uses a focused beam of 30 keV gallium ions to scan the surface of a specimen. The gallium beam at low currents (10-70 pA) can be used to produce images (resolution <100 nm) of the sample via secondary electrons emitted during interactions of the incident ions with the specimen. Alternatively, at high currents (1000-7000 pA), the beam can be used to rapidly sputter away the specimen to expose a cross-sectional surface without the distortion or alteration found in other cross-sectioning techniques. This capability is appropriate in this study to section individual splats and observe microstructural features at the splat-substrate interface. A further capability of the FIB is the ability to produce thin (~100 nm) cross-sectional samples at almost any desired location in a sample, suitable for examination by a transmission electron microscope (TEM). A number of electron transparent sections were prepared through different splats and examined in a Philips CM200 TEM. In addition, a FEI Nova 200 Nanolab dual beam FIB was used to prepare serial sections of images through individual splats. These serial section data sets were used to generate three-dimensional images of the splat-substrate interface. Details of this technique can be found elsewhere (Ref 13).

3. Results and Discussion

The electrochemical method results in a porous oxide, the other a sealed oxide. The hydrothermal oxide thickness was measured using a FIB microscope to be 845 ± 70 nm (as shown in Fig. 1a), while the composition was determined by Ion Beam Analysis (IBA) to be aluminum oxy-hydroxide (AlOOH). The hydrothermal oxide consists of a ~600 nm AlOOH surface layer together with a 245 nm interface layer. The structure of the hydrothermally grown oxide was observed to have fine pore holes (<20 nm) with a smooth external surface. Conversely, the structure of the electrochemically grown oxide has larger pore holes, approximately 50 nm in diameter, in the sectioned surface, together with large pore holes on the external surface 300-600 nm in diameter. The electrochemical oxide thickness was measured in the FIB to be 650 ± 20 nm (as shown in Fig. 1b), and the composition was determined by IBA to be alumina (Al_2O_3). The SEM thickness measurements and the IBA compositions were used to estimate the density values for the hydrothermal oxide (3.2 ± 0.4 g cm^{-3}) and the electrochemical oxide (3.32 ± 0.5 g cm^{-3}). By comparing these estimated densities with the nominal densities of fully dense AlOOH (3.44 g cm^{-3}) and Al_2O_3 (3.985 g cm^{-3}), respectively, estimates of porosity were determined for the hydrothermal oxide (7 ± 12%) and the electrochemical oxide (17 ± 15%).

Data from these two specimens were compared with experiments previously performed on polished aluminum substrates with a native oxide (thickness 10-30 nm) (Ref 14).

3.1 Splats on Hydrothermal Oxide Coating

Investigation of the HVAF thermally sprayed aluminum substrate with a hydrothermal oxide revealed that many particle impacts had occurred but no particles had bonded to the substrate. For example, an overview

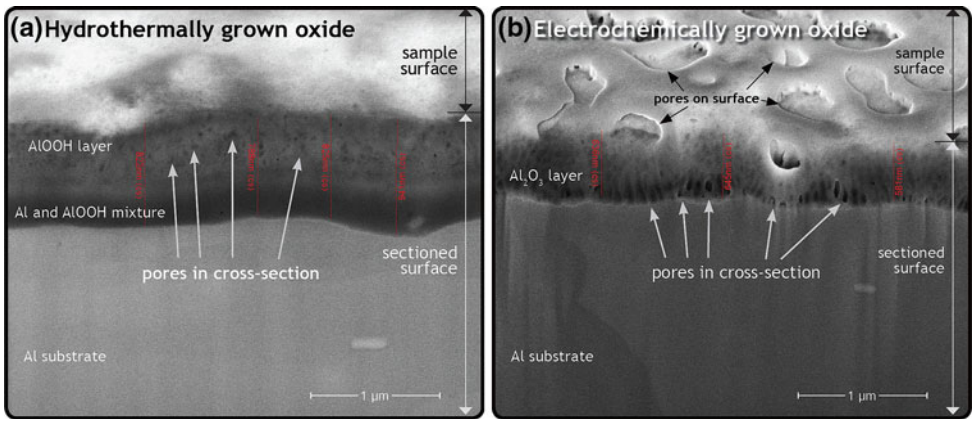

Fig. 1 Oxidized aluminum substrates. (a) FIB sectioned hydrothermally grown oxidized aluminum sample with an oxide layer thickness of 845 ± 70 nm. The oxide consists of a ~600 nm AlOOH surface layer together with a 244 nm interface layer. (b) FIB sectioned electrochemically grown oxidized aluminum sample with a surface oxide layer thickness of 650 ± 20 nm composition of Al_2O_3. (cs) = cross section

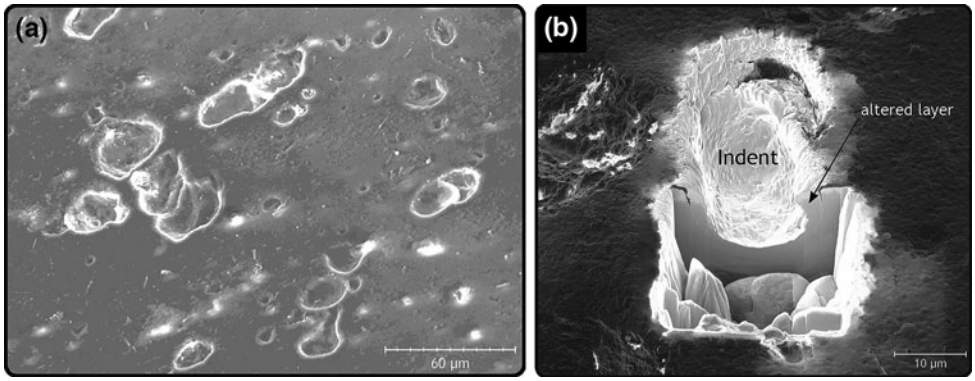

Fig. 2 Only impacts where found on an aluminum substrate with a hydrothermally grown oxide layer thermally sprayed with NiCr particles using the HVAF technique. (a) Secondary electron image of the overall surface area showing indents on the oxidized Al surface. (b) Secondary electron image of a FIB-section through an indentation which shows the effect of an impact on the substrate. The quality of the images was impaired due to charging of the surface oxide

secondary electron image of this sample is shown in Fig. 2(a). A higher magnification cross-sectional image of particle impacts shown in Fig. 2(b) confirms that no particles had bonded to the substrate and that only indents remain. The indent shown in Fig. 2(b) penetrate several microns into the surface. The FIB-sectioned indent shows that the Al substrate and the surface oxide have both been deformed and that the surface oxide remains on the surface of the indent crater. The presence of this oxide was confirmed by energy dispersive x-ray analysis (EDS).

3.2 Splats on the Electrochemical Oxide Coating

Investigation of the aluminum substrate with an electrochemical oxide layer thermally sprayed with the HVAF technique revealed that many NiCr particles had bonded successfully. A variety of splat types and sizes can be observed in the overview image of the sample shown in Fig. 3(a). The splat types observed include: (a) solid, (b) semi-molten, and (c) molten splats as well as indents (where no splat remained after impact). Secondary electron images recorded at higher magnification of indents, solid splats, semi-molten splats, and molten splats are shown in Fig. 3(b-e), respectively.

The HVAF thermally sprayed electrochemically grown oxide layer exhibited a mixture of indents ($18 \pm 4\%$), solid particles ($40 \pm 7\%$), semi-molten ($13 \pm 4\%$), and molten splats ($29 \pm 6\%$). This was based on an examination of 90 splats to derive a statistical breakdown of the different splat types. These values are compared in Table 1 with the percentages of splat types observed on other aluminum substrates, including aluminum with only a native oxide present. The interesting difference between the aluminum substrate with a native oxide and the aluminum substrate with the electrochemically grown alumina oxide layer is the increased percentage of molten splats. The percentage of molten splats observed on the electrochemically oxidized aluminum in this study, is similar to the percentage of molten splats on substrates with a hardness similar to alumina (Al_2O_3: 1700 MPa) observed in the previous study (Ref 15), whereas the percentage of solid splats is closer to that observed on aluminum substrates (Al: 338 MPa). The oxidized surface layer has affected the splat types differently. Molten droplets or solid particles that have become molten during impact, have spread laterally, dissipating energy in a direction parallel to the substrate surface, whereas solid and semi-molten particles have deformed both the surface oxide layer and the underlying aluminum substrate. The amount of deformation caused by solid and semi-molten particles was less on the oxidized layer than the native oxide. In previous studies (Ref 15, 16), the percentage of splat types sprayed onto substrates of different hardnesses was investigated, where it was shown that a larger amount of particle deformation and particle heating occurs in particles during impact on harder substrates. Evidence of particle heating during impact has also been observed recently (Ref 17) for copper particles cold-sprayed onto aluminum substrates.

3.3 Solid Splat-Substrate Interface

To investigate how the substrate surface oxide is displaced during a solid particle impact and how it affects solid splat bonding, two representative individual solid splats, of different sizes, on the electrochemically grown oxide layer were investigated in detail via FIB milling and cross-sectional TEM. Figure 4 shows a series of images of solid splats, of which Fig. 4(a, b) are cross-sectioned solid splats embedded in the substrate with diameters of 15 and 35 µm, respectively. Figure 4(c, d) shows TEM bright field images of the splat-substrate interface at the center and at the periphery of the splat, respectively. The splat is darker because the splat material (NiCr alloy) is denser than the aluminum substrate. Although the oxide shows structure, it was found to be largely amorphous. These images were very surprising as they suggest that the oxide at the splat-substrate interface (under the splat) was plastically deformed without fracturing. This was unexpected because oxides are normally brittle below melting point temperatures. Perhaps the interfacial oxide has been able to plastically deform during high pressures experienced

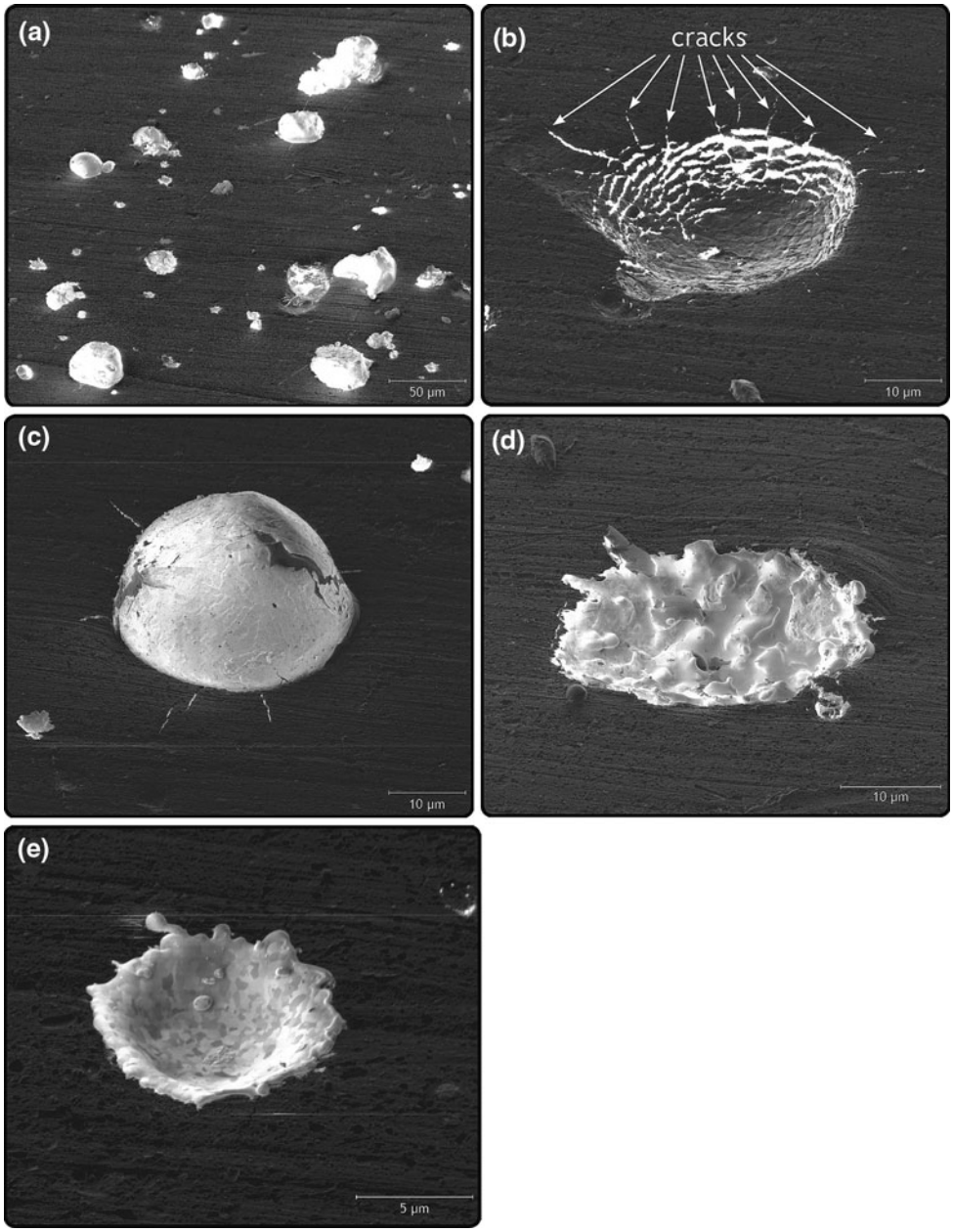

Fig. 3 Impacts and splats where found on the aluminum substrate with an electrochemically grown oxide layer thermally sprayed using the HVAF technique. Secondary electron images show: (a) general area image, (b) an indent where the splat has not remained, (c) solid splat, (d) semi-molten splat, and (e) fully molten splat. The quality of the images was impaired due to charging of the surface oxide

Table 1 Indents and types of splats observed on various aluminum substrates

Al substrate	Number examined	Indents, %	Bonded solid splats, %	Bonded semi-molten splats, %	Bonded molten splats, %
Electrochemical grown oxide layer	90	18 ± 4	40 ± 7	13 ± 4	29 ± 6
Native oxide layer	235	46 ± 4	28 ± 2	25 ± 3	2 ± 1
Hydrothermally grown oxide layer	400	100 ± 5	0 ± 1	0 ± 1	0 ± 1

during impact? Conversely, the oxide beside the splat, shown in Fig. 3(c) shows a brittle nature as cracks can be observed extending radially outward from the splat. The images also suggest that the surface oxide is not removed during the particle impact, but is still present at the interface across the entire splat-substrate interface.

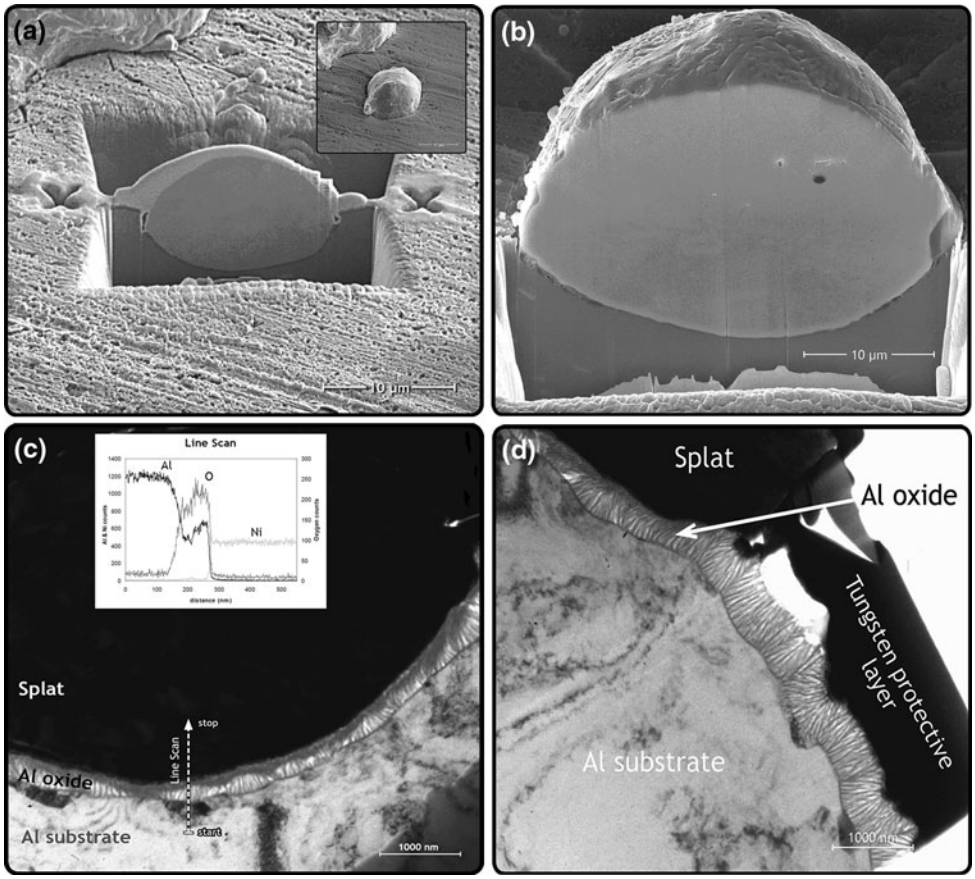

Fig. 4 Solid NiCr splats bonded to an electrochemically oxidized aluminum substrate: (a) 15 μm diameter cross-sectioned solid splat (the inset image is of the splat prior to cross-sectioning), (b) 35 μm diameter cross-sectioned solid splat, (c) TEM bright field image at the center of splat-substrate interface (the inset image is the elemental concentrations of the line scan), and (d) TEM bright field image at the edge of the splat-substrate interface

Table 2 Dimensions and oxide thicknesses for two sectioned splats

Parameter	Splat 1 (Fig. 4a)	Splat 2 (Fig. 4b)
Splat diameter, μm	15 ± 2	35 ± 2
Splat penetration, μm	4.5 ± 0.5	8 ± 0.5
"Postimpact" oxide thickness at splat-substrate interface, nm	100-300	20-150
Preimpact "substrate" oxide thickness, nm	650 ± 20	650 ± 20
Oxide thickness reduction	54-85%	77-97%

The amount of deformation to the substrate can be assessed in the images of the splat cross sections (Fig. 4a and b) which show that the substrate has been deformed inward by approximately 25% of the particle diameter. The dimensions of the splat sizes and oxide thicknesses listed in Table 2 show a relationship between particle impact kinetic energy (pressure) and the thickness of the oxide at the interface. Similarly, the splat cross sections also show the deformation to the impacted particles. The raw powder particles are typically spherical in shape prior to impact, but the splats have a much shallower curvature at the splat-substrate interface compared to the splat curvature on the top surface of the splat.

The amount of deformation to the oxide can be assessed in Fig. 4(c, d) by comparing the thickness of the interfacial oxide directly underneath the splat with the oxide adjacent to the splat. Although the interfacial oxide is still intact, it has been deformed (along with the substrate) and is much thinner due to the impact of the particle. Because of the high deformation of the substrate, the surface area of the oxide at the splat-substrate interface is larger than the surface area of the oxide prior to impact. Hence the oxide is thinner at the splat-substrate interface compared to the original surface oxide thickness (~650 nm). The thickness and uniformity of the original preimpact oxides can be observed in Fig. 1. Variations in thickness of the original oxides are much smaller in scale than the particle dimensions. During impact, the oxide is deformed to be much thinner (20-150 nm in some local regions) underneath the larger diameter splats, compared to the oxide under the smaller 15 μm diameter splat (100-300 nm).

The cross section images in Fig. 4(c and d) also show the structure and local compression of the oxide at the interface. The somewhat porous and needle-like microstructure of the oxide is continuous and is very similar at

both the substrate-splat interface and on the substrate adjacent to the splat. Elemental maps and line scans (e.g., see inset of Fig. 4c) performed using an energy dispersive spectroscopy (EDS) in conjunction with the TEM show that the solid splat-oxide layer interface is chemically abrupt with no evidence of the oxide diffusing into the NiCr splat or vice versa. Hence, no chemical bonding is observed in these samples. The splat has bonded mechanically due to the deformation of the substrate and the surface oxide during the particle impact. The representative solid splats investigated in this section show that the solid splats have deformed, but have not penetrated the oxide. At some locations, the oxide is very thin (≈20 nm) but the oxide is still present between the splat and the substrate material even in these very thin local regions.

3.4 Molten Splat-Substrate Interface

The microstructure of molten splats was also investigated in detail on the electrochemically oxidized aluminum substrate. The molten splat shown in Fig. 5(a) was sectioned using FIB milling to investigate the splat cross section (shown in Fig. 5b). The oxide layer (which exhibits dark contrast in Fig. 5b) has been deformed during the particle impact. This has resulted in specific locations where the splat has penetrated through the oxide layer to make contact with the aluminum metal substrate. FIB/TEM investigations of Ti splats kinetically sprayed onto steel substrates (Ref 18) found similar features in the cross sections images including a thin interfacial (~10 nm) oxide layer at bonding locations.

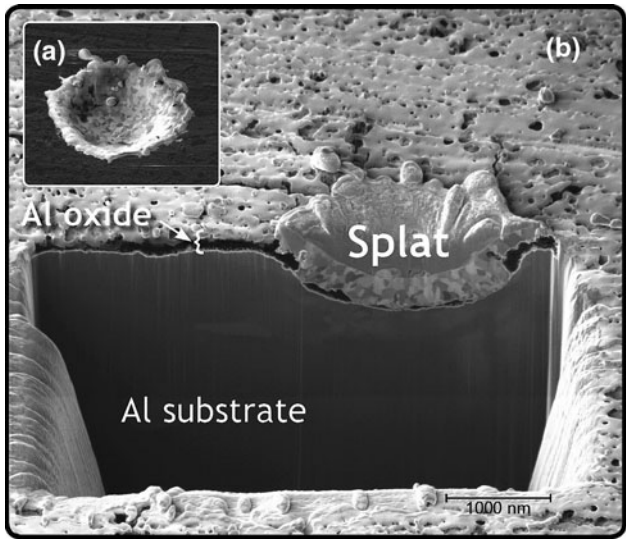

Fig. 5 (a) The inset image is of a molten splat bonded to the electrochemically oxidized aluminum substrate prior to sectioning, (b) FIB cross section of the molten splat which shows how the substrate and the surface oxide have been deformed during the particle impact. The image of the cross section also shows specific locations where the splat has penetrated through the oxide layer to make contact with the underlying aluminum metal substrate

A dual beam FIB has the ability to automatically repeat millings and take images from successive locations in a sample (Ref 13). One hundred "slice and view" images across the molten splat shown in Fig. 6(a) were used to produce 3D reconstructed images of various features in a molten splat, these are shown in Fig. 6(b, c, and d). The 3D reconstructions of the NiCr splat, Al oxide, voids and the Al substrate provide a unique visual aid for investigating the shape and interaction of these features at the interfaces. The underside of the NiCr splat shows a roughened splat surface adjacent to the interface. In particular, the images show that close contact is occurring at the center of the splat, where the impacting particle makes first contact and where most of the momentum is imparted to the substrate. The center of the splat is also where the oxide is most disturbed and where the splat has broken through the oxide layer to make close contact with the metal substrate underneath. Metal-to-metal contact between the splat and the aluminum metal substrate occurs only in regions where the aluminum oxide has been disrupted. Conversely, at the periphery of the splat-substrate interface, voids are located indicating a region of poor bonding. The 3D reconstruction images also show how the oxide at the interface has been deformed and that no significant loss of the oxide has occurred.

These images confirm that molten splats can penetrate into the oxide layer forming strong interlocking bonding features. In comparison, the larger solid splats deformed the substrate and surface oxide to a greater extent, but did not penetrate the surface oxide. From this observation, it is concluded that penetration of the oxide by the smaller molten splats was aided by the molten state of the impacting splat providing enhanced viscous flow during impact.

3.5 Comparison of Hydrothermal and Electrochemical Oxide Coatings

Bonding of splats was observed on electrochemically grown oxide layers (650 nm), but not on hydrothermally grown oxide layers (845 nm). Several differences between the two oxidized substrates may account for this observation. Key differences between these two substrates are discussed in the following sections.

3.5.1 Thickness. The hydrothermally grown (boiled) oxide layer is somewhat thicker (845 ± 70 nm) compared to the electrochemically grown oxide layer (650 ± 20 nm). The effect of the surface oxide on interfacial bonding in high-velocity thermal-spray coatings for solid splat coatings has been discussed by others (Ref 1-3). These researchers have observed that successful particle bonding occurs above certain critical velocities. It has been suggested that fracturing of surface oxide layers on the incident particle and on the substrate becomes a necessary part of coating formation to allow inter-diffusion or metallurgical bonding to occur (Ref 4). This suggests that based on the oxide layer thickness, the thicker hydrothermally grown oxide layers are a larger impediment for splat bonding than the electrochemically grown oxide layers.

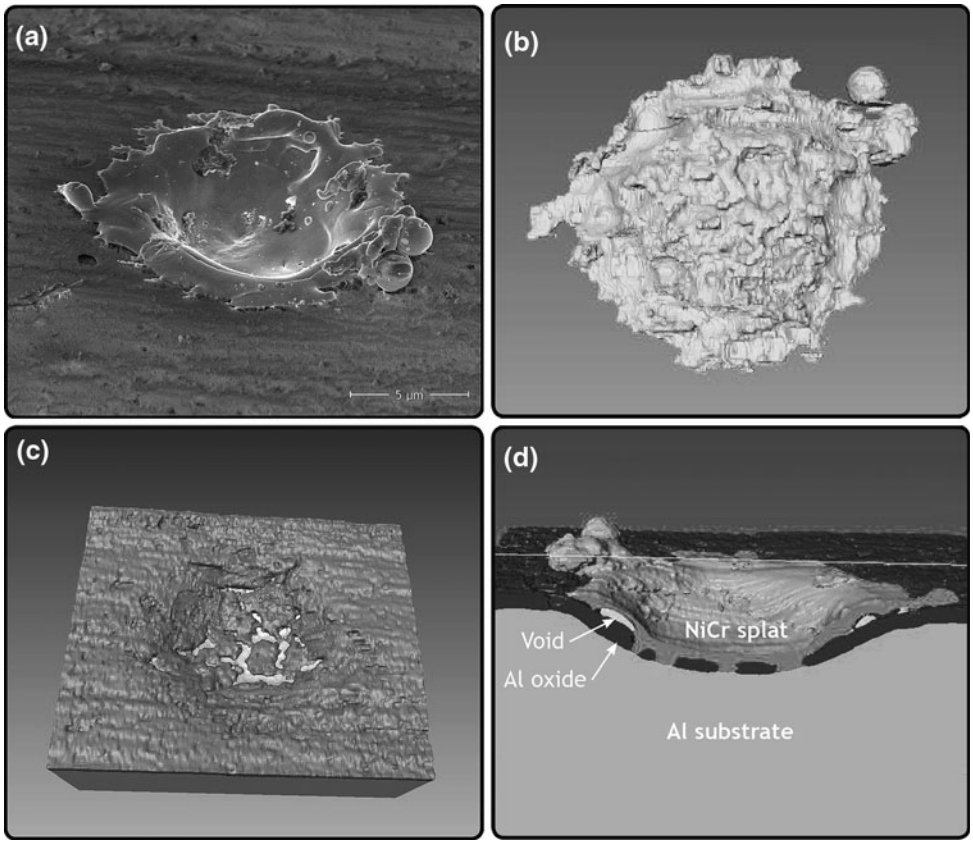

Fig. 6 A 3D reconstruction of a molten NiCr splat on an electrochemically oxidized aluminum substrate. (a) Secondary electron image of the molten splat, (b) reconstructed image of the turbulent underside of the NiCr splat, (c) reconstructed image of the indent oxide layer showing deformation an cracking, and (d) reconstructed image of the splat-substrate cross section showing locations where the splat material has penetrated the interfacial oxide

3.5.2 Microstructure. The electrochemical method produces a porous oxide (porous volume = 17 ± 15%), whereas the hydrothermal method a sealed oxide (porous volume = 7 ± 12%). The differences in oxide microstructure affect the hardness of the oxide. The hardness of the oxide, in turn, affects the ability of the incident particle to fracture and penetrate the oxide layer to allow interdiffusion or metallurgical bonding to occur. The low porosity of the hydrothermally grown oxide layers would therefore be more resistant to fracturing and penetration compared to the electrochemically grown oxide, which has a significantly higher porosity.

3.5.3 Composition. The composition of the hydrothermally grown oxide has been determined to be AlOOH. Upon heating, AlOOH looses water and forms Al_2O_3. The temperature range of this transition is between 440 and 1200 °C (Ref 19).

$$4AlOOH \rightarrow 2Al_2O_3 + 2H_2O$$

The image in Fig. 2(b) of a sectioned indent in the hydrothermally grown oxide layer shows a 1-2 μm thick layer on the surface of the indent. This layer may be due to a loss of water during particle impact. The oxide decomposition, loss of water, and gas release upon heating during particle impact could affect the ability of a particle to penetrate the oxide and bond to the metal substrate underneath.

4. Conclusions

The experiments in this study showed that the thickness and composition of substrate surface layers strongly influenced the ability of splats to bond to a substrate. No splats were found on the aluminum oxy-hydroxide oxide layer (845 nm), whereas bonding did occur on an alumina layer (650 nm) grown on an aluminum substrate. Bonded splats on the alumina substrate were investigated in more detail. Cross sections of solid splats showed that the aluminum substrate and surface oxide had been deformed during the particle impact. This has resulted in some locations where the oxide was as thin as 20 nm but was still present between the splat and the substrate even in these very thin local regions. Cross-sectional measurements of molten particles show that the oxide has been penetrated in several locations allowing close proximity of the splat metal to the substrate metal to occur. The penetration of the oxide by the smaller molten splats was aided by the molten state of the impacting splat providing

enhanced viscous flow during impact. Images of the interfacial oxide for both solid and molten splats were very surprising as they suggest that the oxide is not removed but had been plastically deformed during impact.

FIB ''slice and view'' images, plus 3D reconstructions of the interfacial oxide, showed that no significant loss of oxide had occurred from the substrate, and there was no evidence of diffusion of the oxide into the NiCr splat. During the particle impact, the oxide and underlying substrate are deformed. The deformation had the effect of spreading the surface oxide over a larger surface area (compared to the preimpact surface area). This allowed small-scale redistribution and penetration of the oxide material by a molten splat, making it possible for metal-to-metal contact to occur and possibly metallic or metallurgical bonding. The cross-sectional profile of the interfacial oxide penetrations show that they provide mechanical interlocking features for bonding the molten splat to the substrate.

These results confirm that successful bonding occurs only when the substrate and surface oxide are significantly deformed to produce mechanically interlocking features. In the case of smaller molten splats, less substrate deformation had occurred but in some locations the oxide layer had been disrupted to allow possible metallurgical bonding and provide additional mechanically interlocking features.

Acknowledgments

The authors thank Steve Mathews previously of Auckland University and Holsters Engineering in Tokoroa for assistance with HVAF thermal spray sample preparation.

References

1. T.H. Van Steenkiste, J.R. Smith, and R.E. Teets, Aluminum Coatings Via Kinetic Spray with Relatively Large Powder Particles, *Surf. Coat. Technol.*, 2002, **154**(2-3), p 237-252
2. M. Grujicic, J.R. Saylor, D.E. Beasley, W.S. DeRosset, and D. Helfritch, Computational Analysis of the Interfacial Bonding Between Feed-Powder Particles and the Substrate in the Cold-Gas Dynamic-Spray Process, *Appl. Surf. Sci.*, 2003, **219**, p 211-227
3. K. Kang, S. Yoon, Y. Ji, and C. Lee, Oxidation Dependency of Critical Velocity for Aluminum Feedstock Deposition in Kinetic Spraying Process, *Mater. Sci. Eng.*, 2008, **A486**, p 300-307
4. T.H. Van Steenkiste, J.R. Smith, R.E. Teets, J.J. Moleski, D.W. Gorkiewicz, R.P. Tison, D.R. Marantz, K.A. Kowalsky, W.L. Riggs, II, P.H. Zajchowski, B. Pilsner, R.C. McCune, and K.J. Barnett, Kinetic spray coatings, *Surf. Coat. Tech.*, 1999, **111**, p 62-71
5. P. Fauchais, M. Fukumoto, A. Vardelle, and M. Vardelle, Knowledge Concerning Splat Formation: An Invited Review, *J. Therm. Spray. Technol.*, 2004, **13**(3), p 337-360
6. W.J. Trompetter, A. Markwitz, and M. Hyland, Use of IBA Techniques to Characterize High Velocity Spray Coatings, *Modern Phys. Lett.*, 2001, **B15**, p 1428-1436
7. W.J. Trompetter, A. Markwitz, and M. Hyland, Role of Oxides in High Velocity Thermal Spray Coatings, *Nucl. Instrum. Method*, 2002, **B190**, p 518-523
8. S. Lopez, J.P. Petit, H.M. Dunlop, J.R. Butruille, and G. Tourillon, Acid-Base Properties of Passive Films on Aluminum: I. A Photoelectrochemical Study, *J. Electrochem. Soc.*, 1998, **145**(3), p 823-829
9. S. Wernick, R. Pinner, and P. Sheasby, *The Surface Treatment and Finishing of Aluminum and Its Alloys*, 5th ed. Vol 1 and 2, ASM International, Materials Park, OH, 1987, p 661
10. J.A. Browning, Hypervelocity Impact Fusion—A Technical note, *J. Therm. Spray. Technol.*, 1992, **1**(4), p 289-292
11. N. Rowlands and P. Munroe, FIB for the Evaluation of Non-Semiconductor Materials, *Microstr. Sci.*, 1998, **26**, p 26-29
12. J.M. Cairney, R.D. Smith, and P.R. Munroe, Transmission Electron Microscope Specimen Preparation of Metal Matrix Composites Using the Focused Ion Beam Miller, *Microsc. Microanal.*, 2000, **5**, p 452-462
13. M.D. Uchic, L. Hozler, B. Inkson, E.L. Principe, and P.R. Munroe, 3D Microstructural Characterisation Using Focused Ion Beam Tomography, *MRS Bull.*, 2007, **32**, p 408-416
14. W.J. Trompetter, M. Hyland, P. Munroe, and A. Markwitz, Evidence of Mechanical Interlocking of NiCr Particles Thermally Sprayed onto Al Substrates, *J. Therm. Spray. Technol.*, 2005, **14**(4), p 524-529
15. W.J. Trompetter, M. Hyland, P. Munroe, D. McGrouther, and A. Markwitz, The Effect of the Substrate Hardness on Particle Morphology in High Velocity Thermal Spray Coatings, *J. Therm. Spray. Technol.*, 2006, **15**(4), p 663-669
16. G. Bae, Y. Xiong, S. Kumar, K. Kang, and C. Lee, General Aspects of Interface Bonding in Kinetic Sprayed Coatings, *Acta Mater.*, 2008, **56**, p 4858-4868
17. P.C. King, S.H. Zahiri, and M. Jahedi, Focused Ion Beam Micro-Dissection of Cold-Sprayed Particles, *Acta Mater.*, 2008, **56**, p 5617
18. K.H. Kim, M. Watanabe, K. Mitsuishi, K. Iakoubovskii, and S. Kuroda, Impact Bonding and Rebounding Between Kinetically Sprayed Titanium Particle and Steel Substrate Revealed by High-Resolution Electron Microscopy, *J. Phys. D Appl. Phys.*, 2009, **42**, p 065304
19. J.G. Li and X. Sun, Synthesis and Sintering Behavior of a Nanocrystalline α-Alumina Powder, *Acta Mater.*, 2000, **48**(12), p 3103-3112